



Article

PLLA Nanosheets for Wound Healing: Embedding with Iron-Ion-Containing Nanoparticles

Aslan Mussin¹, Ali A. AlJulaih¹, Neli Mintcheva^{1,2}, Delvin Aman³, Satoru Iwamori^{1,4}, Stanislav O. Gurbatov⁵, Abhishek K. Bhardwaj⁶ and Sergei A. Kulinich^{1,4,*}

¹ Department of Mechanical Engineering, Tokai University, Hiratsuka, Kanagawa 259-1292, Japan

² Department of Chemistry, University of Mining and Geology, 1700 Sofia, Bulgaria

³ Catalysis Division, Petroleum Refining Department, Egyptian Petroleum Research Institute, Cairo 11727, Egypt

⁴ Research Institute of Science and Technology, Tokai University, Hiratsuka, Kanagawa 259-1292, Japan

⁵ Institute of Automation and Control Processes, Far Eastern Branch, Russian Academy of Science, Vladivostok 690041, Russia

⁶ Department of Environmental Science, Amity University, Gwalior 474005, Madhya Pradesh, India

* Correspondence: skulinich@tokai-u.jp

Abstract: This article reports on polymer (PLLA, poly(L-lactic acid)) nanosheets incorporated with Fe-ion nanoparticles, aiming at using the latter nanoparticles as a source to release Fe ions. Such Fe ions should facilitate burn wound healing when such nanosheets are applied as a biomedical tissue on skin. Laser ablation in liquid phase was used to produce Fe-containing nanoparticles that, after incorporation into PLLA nanosheets, would release Fe ions upon immersion in water. Unlike most iron-oxide nanostructures, which are poorly soluble, such nanoparticles prepared in chloroform were found to have water solubility, as they were shown by XPS to be based on iron chloride and oxide phases. After incorporation into PLLA nanosheets, the ion-release test demonstrated that Fe ions could be released successfully into water at pH 7.4. Incorporation with two different metal ions (Fe and Zn) was also found to be efficient, as both types of ions were demonstrated to be released simultaneously and with comparable release rates. The results imply that such polymer nanosheets show promise for biomedical applications as potential patches for healing of burns.

Keywords: PLLA nanosheets; laser ablation in liquid; Fe-containing nanoparticles; metal-ion release; burn wound healing



Citation: Mussin, A.; AlJulaih, A.A.; Mintcheva, N.; Aman, D.; Iwamori, S.; Gurbatov, S.O.; Bhardwaj, A.K.; Kulinich, S.A. PLLA Nanosheets for Wound Healing: Embedding with Iron-Ion-Containing Nanoparticles. *Nanomanufacturing* **2023**, *3*, 401–415. <https://doi.org/10.3390/nanomanufacturing3040025>

Academic Editors: Wenjie Zhou and Sotirios Baskoutas

Received: 4 August 2023

Revised: 20 September 2023

Accepted: 12 October 2023

Published: 19 October 2023



Copyright: © 2023 by the authors. Licensee MDPI, Basel, Switzerland. This article is an open access article distributed under the terms and conditions of the Creative Commons Attribution (CC BY) license (<https://creativecommons.org/licenses/by/4.0/>).

1. Introduction

Wounds are defined as damage or disturbance of normal anatomical structure and function of skin resulted from pathological processes that begin internally or externally [1,2]. Among different types of wounds, burns are known typically to need long-lasting and complex treatment to provide, support and accelerate their healing [3–13]. An ideal wound dressing used for their treatment should accelerate one or several stages of the healing processes, including the inflammatory phase, the migratory phase, the proliferative phase and the remodeling phase. Nowadays, a variety of wound dressings are available and still widely used to treat such wounds [3–10,12,13]. However, even though the characteristics of “ideal” dressings for wound treatment are well known, such ultimate dressings are still difficult to realize within the same material [4–13]. It is still challenging, if ever possible, to realize an optimal combination of desired properties in one wrapping material, implying that new materials with improved characteristics are still highly anticipated. In parallel, incorporation of metal ions such as Mg, Zn, Fe and Cu is believed to be beneficial for efficient wound healing [2,4,5,11,14–16]. However, very little progress has been achieved in this direction thus far.

Free-standing ultra-thin films (also known as nanosheets, NSs) of several biodegradable polymers (e.g., poly(L-lactic acid), PLLA) have been recently reported as efficient materials to cover burns, with the ability to adhere to any shape and protect wounds for days without the need for daily replacement [11,17–20]. As wound wrapping materials, such NSs are: (1) inexpensive and relatively easy to prepare; (2) highly adhesive to virtually any surface with any shape; (3) permeable to water and air and biodegradable; (4) good as barriers for infection and dirt, and so on [11,17–20]. Embedding such inexpensive and biodegradable polymer NSs with ions of crucial metals that can be released upon contacting the wound surface is therefore believed to enhance further their performance as burn-wound dressings [11,17–20].

Embedding PLLA nanosheets with sources of metal ions, such as Mg, Zn, Fe and Cu, is believed to provide additional merits to such biomedical materials as, these ions were reported to be essential for improved wound healing [2,11,14–16]. In our previous work, we prepared PLLA NSs incorporated with Zn-containing NPs and demonstrated that NPs based on both ZnCl_2 and ZnO can be efficient sources of Zn ions that can be released from PLLA NSs in contact with a water medium [11]. Since embedded NPs should be sufficiently soluble in water, we used ZnO - and ZnCl_2 -based NPs which were then incorporated into PLLA NSs by means of spin-coating. The produced NSs were characterized, and their ability to release Zn ions was tested after immersion in water at pH of 7.4 and 37°C [11]. To prepare such Zn-containing NPs, we applied laser ablation in liquid (LAL) phase, which is a convenient laboratory technique to prepare diverse nanomaterials (including metallic and metal oxide NPs, among others) with easy parameter control and at laboratory scale [21–35] (see Figure 1).

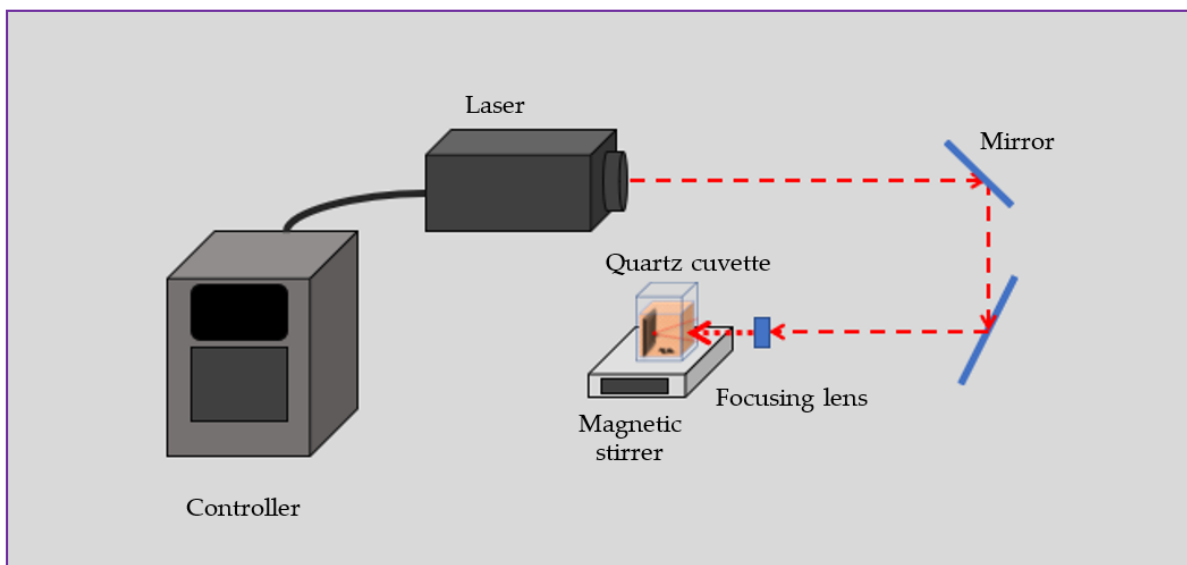


Figure 1. Setup with ns-pulsed laser used to produce nanoparticles via ablating iron plate in chloroform.

Encouraged by the previous results, herein we apply the same method to produce Fe-containing NPs as nano-reservoirs for Fe ions that can be released from their PLLA matrix (NSs) upon embedment. We also employed LAL in chloroform to produce Fe-containing NPs, expecting such NPs to be based on chloride phases, similar to our previous work on Zn ablation in chloroform [11]. When LAL is applied to Fe targets in water or air, the product is known to be based on various iron oxides/hydroxides [22,33,34,36–40]. Based on the literature, all major Fe oxides are known to be insoluble in water, which is why we decided to rely on Fe chloride-based nanomaterials, whose formation was expected as a result of Fe ablation in chloroform.

Thus, this work took advantage of LAL as a method to prepare Fe-containing NPs which are soluble in water. Two types of Fe-Cl NPs were prepared at different laser

parameters and then characterized, after which they were incorporated into PLLA NSs. For comparison, we also used commercially available iron oxide NPs (Fe_2O_3), which were also embedded into PLLA nanosheets. As a next stage, we studied how the prepared NSs released Fe ions, the dynamics that should be of high importance when such biomedical materials are applied for wound healing. Finally, we demonstrated NSs incorporated with two types of NPs that contain two metal ions (Fe and Zn), as well as their ion release.

Hence, the work paves an avenue for easy-to-prepare and low-cost new-generation biomedical materials, i.e., bio-friendly polymer nanosheets incorporated with nano-containers that can release metal ions, thereby accelerating wound healing. Such materials are highly anticipated for multiple biomedical applications, especially as inexpensive wound-dressing in surgery and regenerative medicine.

2. Experimental Part

2.1. Chemicals and Materials

Iron plates (99.8% pure) were supplied by Nilaco Corp. Deionized water, chloroform (99.0% pure) and ethanol (99.5%) were all purchased from Wako Pure Chemical Industries (Japan). Phosphate-buffered saline solution (PBS) was purchased from Merck, polyvinyl alcohol (PVA) was acquired from Kanto Chemical Co. (Tokyo, Japan), while Fe_2O_3 and ZnO NPs (with sizes below 50 nm and 20–25 nm, respectively) were supplied by Sigma-Aldrich (Burlington, VT, USA) and Wako Pure Chemical Industries (Osaka, Japan), respectively. Finally, PLLA (Mw: 80–100 kDa) was supplied by Polysciences, Warrington, PA, USA.

2.2. Preparation of Fe-Containing NPs

Laser ablation in liquid (LAL) is a convenient laboratory technique to generate NPs with different morphology, sizes and chemistry [21–29,33,34,41–44]. In this method, a laser beam is typically focused on a solid target (or powder dispersed in liquid), and its pulses ablate (or modify) the target to produce nanostructures with morphology, size and chemistry that depend on the liquid and target used, as well as on the properties of the laser pulses applied [21,24–29,31–34,45]. This approach is attractive for research purposes, since it is simple in use, inexpensive and consumes minimum chemicals, among other advantages. In this study, as we needed water-soluble NPs containing Fe ions, we applied LAL to ablate iron plate in chloroform, as this was expected to result in chloride-based NPs.

Unlike our previous work on ZnCl_2 -based NPs generated via LAL [11], here we applied a nanosecond pulsed laser to ablate iron plates in chloroform. Samples A and B were prepared using a YAG laser operating at different pulse energies, as described in Table 1.

Table 1. Description of Fe-containing colloids produced by ablating iron plate with ns-pulsed laser.

Sample	Ablation Time (min)	Liquid Medium	Pulse Energy (mJ)
Sample A	20	Chloroform	30
Sample B	20	Chloroform	120

Iron metal plate with a thickness of 1.0 mm was cut into pieces $1.5 \times 3.0 \text{ cm}^2$ in size which were then sonicated in ethanol for 5 min. After drying in air, the plates were placed in a quartz cuvette with 15 mL of chloroform. During ablation for 20 min, the produced colloids were magnetically stirred (Figure 1). A nanosecond pulsed Nd: YAG laser with the fundamental wavelength of 1064 nm was used for preparing iron chloride-based NPs. The experimental setup is shown in Figure 1, while more details on both the setup and laser used can be found elsewhere [11,27,32,41,42].

2.3. Characterization of Prepared NPs

The prepared colloids of Fe-Cl-containing NPs were first centrifuged at 16,000 rpm and then drop-cast on Si wafers, for X-ray photoelectron spectroscopy (XPS) and X-ray diffraction (XRD) analyses, or on C-coated Cu grids for transmission electron microscopy (TEM).

Morphology of obtained NPs and NSs were taken using scanning electron microscopy (SEM, S4800 from Hitachi, Tokyo, Japan), while XPS analysis was carried out on a PHI-1600 spectrometer (Physical Electronic Industries, Chanhassen, MN, USA). The recorded binding energy peaks were all corrected for charge shifting by referencing to the adventitious carbon C 1s line at 284.8 eV. In order to remove adventitious carbon from the sample surface, argon sputtering was applied, after which samples were analyzed. Quantification of the peaks was carried out by using the XPSpeak4.1 software, which enabled us to curve-fit the peaks of elements by comparing them with data already available in the literature.

TEM analysis was performed on an HF-2200 tool from Hitachi. The samples were prepared by pipetting as-prepared dispersions onto copper micro-grids and drying in air. The optical characteristics of NPs in colloids were studied using an UV-visible absorption spectroscope (UV-2450, Shimadzu, Kyoto, Japan). The NP size in the liquid state was measured using a nanoparticle analyzer by dynamic light scattering (DLS) technique.

2.4. Nanosheets Loaded with NPs and Their Analysis

Because chloroform is compatible as solvent for our spin-coating-based approach to prepare PLLA NSs, NPs prepared in chloroform were ready for direct mixing with PLLA polymer followed by spin-coating [11,19,20]. Commercial Fe₂O₃ or ZnO NPs used for comparison, prior to further processing, were weighed and dispersed in chloroform, after which they were mixed with PLLA for further spin-coating as PLLA NSs.

Figure 2 shows schematically how NP-embedded PLLA NSs were prepared. NP dispersions in polymer solution of CHCl₃ were spin-coated onto a Si wafer coated with a water-soluble polymer, PVA. After fast immersion in water, free-standing PLLA NSs were delaminated as the PVA dissolved in water. The amount of Fe-containing NPs in the PLLA-CHCl₃ solution was evaluated based on the weight loss of the Fe plate, evaluated after ablation. Because the produced NPs had a complex composition and had both Fe(II) and Fe(III) species, for simplicity, we used concentrations in moles per liter (of Fe atoms) to prepare PLLA NSs embedded with NPs from Samples A and B. If necessary, the as-prepared dispersions were diluted with chloroform to adjust their concentrations prior to mixing with PLLA and further spin-coating.

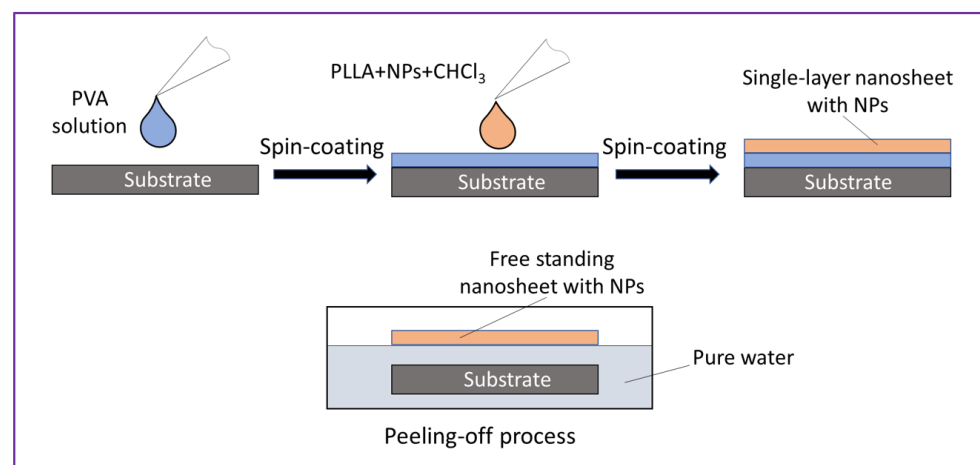


Figure 2. Fabrication of PLLA nanosheet incorporated with nanoparticles.

As seen in Figure 2, the PLLA NSs were prepared by spin-coating. For that, typically the concentration of mixture used was 10 mg of PLLA (as crystals) and 1 mL of LAL-generated colloid. The substrate was spun for 20 s and dried on a hotplate at 70 °C for 90 s.

By using a cutter, a light cut was then made on the substrate to form a sample of $3 \times 3 \text{ cm}^2$, after which the substrate was immersed in water, where it was moved from time to time with tweezers until the PLLA NS began to float (Figure 2). At this point, the pill-off NP-incorporated NS was transferred onto a polyester mat (filter) to preserve its shape and for further storage (see Figure 3c).

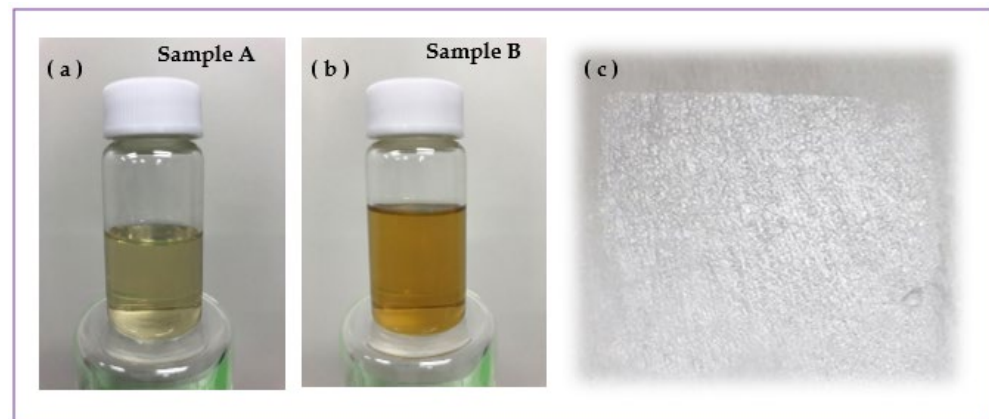


Figure 3. Colloids of Fe-containing NPs laser-generated in chloroform at 30 (a) and 120 mJ/pulse (b), and a PLLA nanosheet incorporated with such NPs (c) placed on polyester filter mat. The actual size of the NS in panel (c) is $3 \text{ cm} \times 3 \text{ cm}$.

2.5. Ion Release from NP-Embedded NSs

Release of metal ions from NS samples was studied by means of inductively coupled plasma mass spectroscopy (ICP-MS). The samples were immersed in flasks with 40 mL of PBS solution (pH 7.4) at 37°C to simulate human body conditions (see Figure 4). To analyze the concentration of Fe ions over time, aliquots of 1 mL were taken and analyzed after certain periods of time. To determine the concentration of metal ion in the analyzed solution, calibration curves were plotted for each analyzed element using standard solutions, as previously reported elsewhere [46–48]. After each sampling, a volume of 1 mL of PBS was added to the sample. For each sample, measurements were carried out in triplicate, after which the obtained results were averaged. Nanosheets incorporated with laser-ablated Fe-containing NPs, as well as their counterparts incorporated with commercially available ZnO and Fe_2O_3 NPs, were evaluated in terms of Fe or/and Zn ion release.

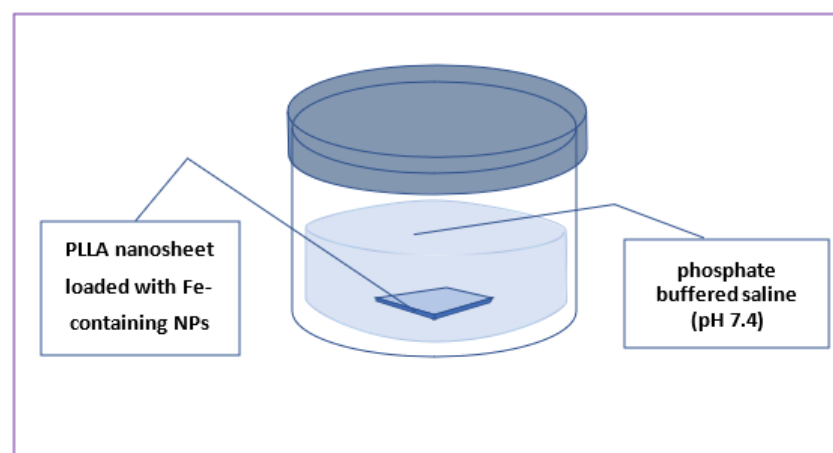


Figure 4. Experimental set-up used for ion-release test.

3. Results and Discussion

3.1. Fe-Containing NPs Prepared by LAL

Figure 3a,b shows the as-prepared colloids of Samples A (a) and B (b), while Figures 5 and 6 exhibit electron microscopy images of the same samples. As well seen in Figure 3a,b, yellow-brownish colloidal dispersions were obtained as a result of iron plate ablation in chloroform. The color of prepared colloids was predictably dependent on the applied laser parameters, which is probably explained by the number, size and chemical composition of produced NPs. No significant temperature increase was detected during the whole ablation process, which agrees well with the literature (as ns-long pulses are known not to transfer much energy to the target and liquid medium [32,41,42]). Since Sample B was prepared using a laser beam with a higher pulse energy, it is reasonable that the concentration of produced NPs should be higher, in agreement with the material loss observed by weighing the iron plates after ablation in both cases.

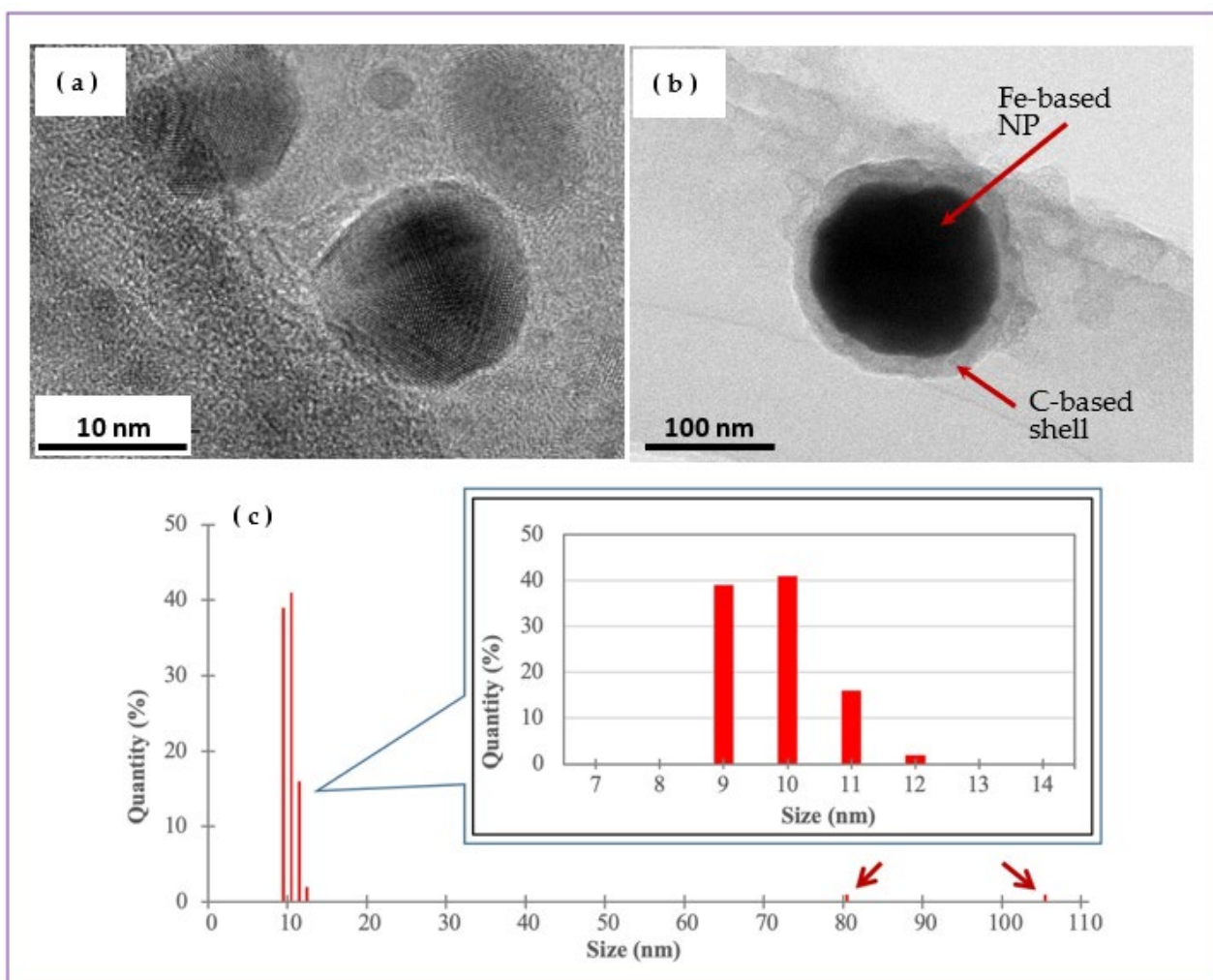


Figure 5. (a,b) TEM images of Fe-based NPs prepared at 30 mJ/pulse (Sample A): (a) small NPs and (b) larger NP with C-based shell. (c) Histogram of size distribution of Fe-containing NPs as measured by DLS. The two red arrows in panel (c) indicate bars for NPs with sizes ~81 and ~106 nm.

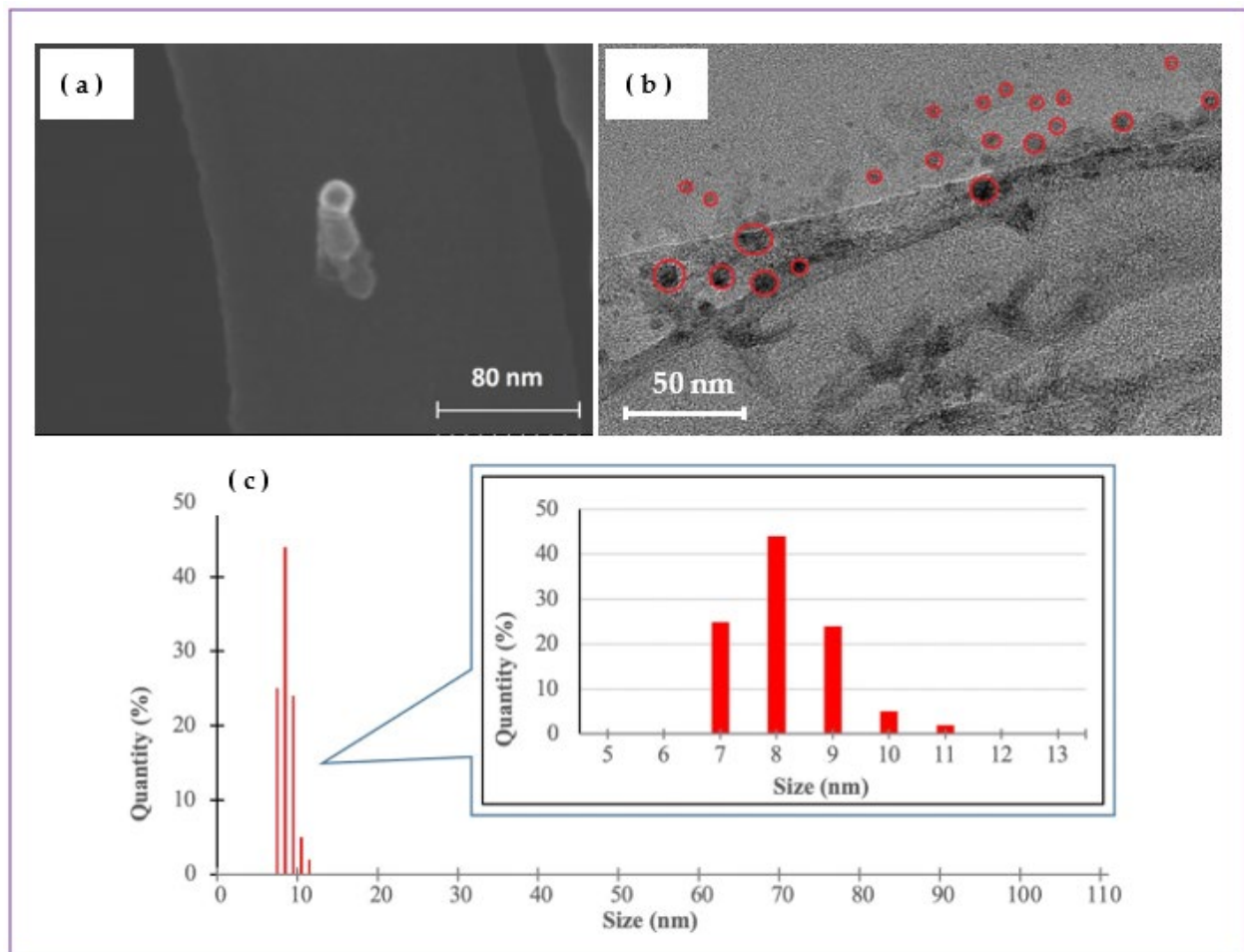


Figure 6. SEM (a) and TEM (b) images of Fe-based NPs prepared at 120 mJ/pulse (Sample B). (c) Histogram of size distribution of NPs in Sample B, as measured by DLS.

Transmission electron microscopy was used to visualize the morphology and size distribution of generated NPs. It is seen that that Sample A prepared at 30 mJ/pulse had spherically shaped NPs with sizes mainly between 7 and 12 nm, with an average size around 10 nm (Figure 5c). At the same time, a small fraction of larger NPs with sizes of 80–105 nm was also observed, as shown by the arrows in Figure 5c. A graphite-like shell surrounding the core of some Fe-based NPs could be observed around larger NPs (Figure 5b), which is believed to be explained by the pyrolysis of chloroform (as the organic medium used), as high temperatures were reached locally in the ablation zone shortly after laser pulses hit the target.

Figure 6 shows that Fe-based NPs in Sample B (prepared at 120 mJ/pulse) had approximately the same sizes as their counterparts produced at a lower pulse energy (30 mJ/pulse), being mainly within the range of 5–15 nm and with an average size of 10 ± 2 nm (Figure 6c). The NPs were also spherically shaped; however, no larger NPs of ~100 nm in size and with well-defined carbon-based shells were found in this sample. The absence of larger NPs in the product produced at a higher pulse energy is not clear yet, as the entire mechanism of NP formation caused by ns-long laser pulses in a chloroform medium is still to be studied. At this stage, we can postulate that probably larger Fe-based NPs formed during ablation could be fragmented by secondary irradiation, as higher energy fluence was used to produce Sample B.

DLS is a technique that permits the evaluation of the size distribution of NPs in dispersions. In Figures 5c and 6c, one can see the histograms of size distribution of NPs in Samples A and B, respectively. The sizes of most NPs in Figure 5c are seen to be within

the range of 9–12 nm, while there is still a small number of NPs with sizes between 80 and 105 nm. This agrees well with the TEM images presented in Figure 5a,b. For Sample B, its NPs are seen in Figure 6c to be somewhat smaller, within the range of 7 to 11 nm, which is also consistent with the TEM and SEM images in Figure 6a,b. Importantly, comparison of Figures 5 and 6 also permits the conclusion that both samples consisted of NPs with sizes proper for embedment into PLLA NSs (which are typically thinner than 100 nm).

UV-visible absorption spectroscopic measurements were carried out on freshly prepared colloids. Typically, Fe-based NPs are known not to be easily identified by UV-visible spectroscopy because they lack sharp absorption bands in this spectral range [49], which makes accurate identification of NP forms by UV-visible spectra difficult. However, both samples are seen in Figure 7 to demonstrate absorption edge at wavelengths below 400 nm, which is consistent with the optical spectra of most oxidized iron phases (Figure 7) [50].

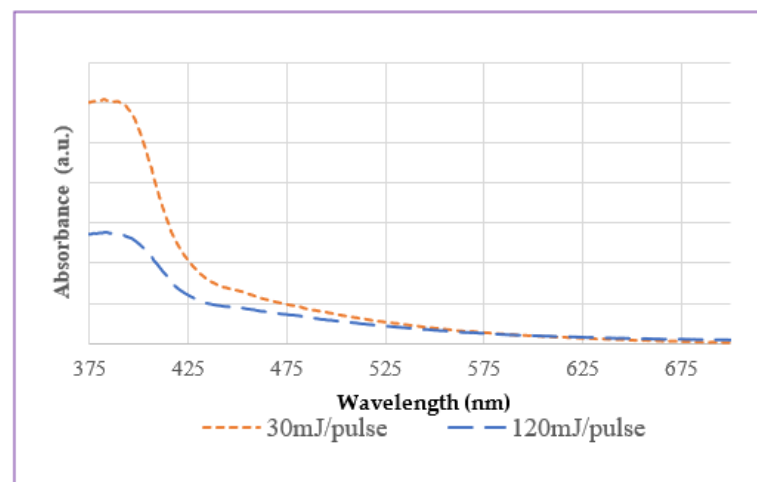


Figure 7. UV-visible spectra of Fe-based colloids prepared using ns-pulsed laser at 30 (orange) and 120 mJ/pulse (blue).

3.2. XPS Analysis of Prepared NPs

Figure 8 presents XPS Fe 2p spectra of Samples A (a) and B (b). Corresponding Cl 2p and O 1s spectra are shown in Supplementary Materials Figures S1 and S2, respectively. As iron is a transition metal, the Fe 2p spectra of both samples presented in Figure 8a,b demonstrate doublets, i.e., peaks at Fe 2p_{3/2} (between ~705 and ~723 eV) and Fe 2p_{1/2} (between ~718 and ~735 eV). For brevity and convenience, below we only focus on the Fe 2p_{3/2} peaks which are easier to analyze and thus are more informative.

Figure 8a presents the Fe 2p spectrum of Sample A, which was curve-fitted using several components. The peak at a lower binding energy (~708 eV) was assigned to metallic iron (Fe(0)), thus implying that the produced NPs were partially composed of non-oxidized metallic iron. It is reasonable to assume that: (i) the liquid medium we used (chloroform) is not a strong oxidizer; (ii) the graphitic shell found in TEM images to surround the core of some NPs could prevent their core from further oxidation; (iii) some metallic phase inclusions could also be embedded by NPs free of graphite shell too. This can explain the presence of Fe(0) species in the produced NPs where they could be distributed at intergranular boundaries or inside amorphous phases of the latter particles. The wide peak observed between 709 and 715 eV was fitted with several components corresponding to Fe-Cl and Fe-O species. Note that, because of the close positions of Fe(II) and Fe(III) species (both oxides and chlorides), it was impossible to distinguish with certainty which of the two (or both) was present and dominated in the sample [22,33,34,37–40].

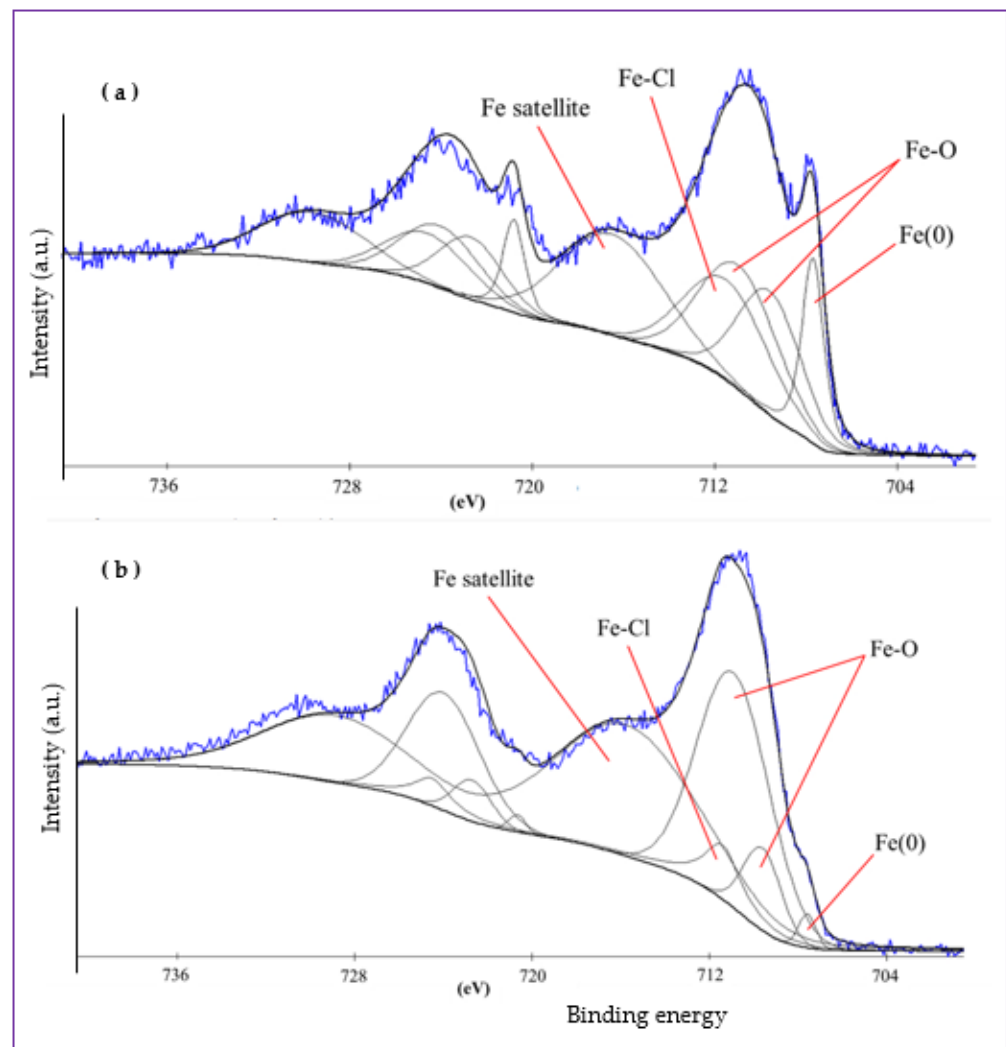


Figure 8. XPS Fe 2p spectra of Samples A (a) and B (b) prepared at 30 and 120 mJ/pulse, respectively. The blue curves present actual measured signal while the black curves are from curve-fitting.

In Figure 8b, the XPS Fe 2p spectrum of Sample B produced via ablation at 120 mJ/pulse is shown. In comparison with Figure 8a, the amount of metallic Fe in this sample is smaller than in its counterpart ablated at 30 mJ/pulse. This was expected, as Fe(0) species are more likely to be oxidized when iron plate is ablated by pulses with higher energy, which should generate higher temperatures in the ablation zone. Moreover, the amount of oxidized forms of iron increases at increased laser energy applied during ablation. In Figures S1a and S2a, Cl 2p and O 1s spectra of Samples A are presented, respectively. In both spectra, it is well seen that the peaks of Fe-Cl and Fe-O compounds are more intense than those of organic C-Cl and C-O species. This agrees well with the above-discussed Fe spectrum of this sample (see Figure 8a), where Fe-Cl and Fe-O species were also detected. On the other hand, since the sample was prepared in chloroform, after which its NPs were drop-cast and kept in the air, the presence of organic C-Cl and C-O species on its surface was also expected.

Similarly, Cl 2p and O 1s spectra of Sample B prepared by ablation at 120 mJ/pulse are presented in Figures S1b and S2b. Here again one can observe intense peaks of Fe-O and Fe-Cl species as dominating components, which agrees well with the above-presented XPS Fe 2p spectrum (Figure 8b). The amount of organic C-Cl species is smaller in this sample, which is probably related to a smaller amount of chloroform absorbed on its surface.

Based on the above-discussed XPS spectra, the NPs of both LAL-prepared samples are composed of a mixture of iron oxide and chloride phases, with a small fraction of metallic Fe phase inclusions. Quantitative analysis made by means of XPS demonstrated that the

overall composition of both samples was very similar, as they had very close contents of iron, chlorine and oxygen (see Supplementary Materials Figure S4). Thus, based on their composition (metallic iron, iron oxide and iron chloride species as main components), NPs of both samples are expected to be somewhat soluble and release Fe ions in contact with water. Thus, such NPs were concluded to be suitable for embedding into PLLA NSs.

3.3. XRD Analysis of Prepared NPs

XRD analysis was performed on the as-prepared Fe-containing NPs to examine their phase composition, with diffraction patterns of the samples being presented in Figure 9. Because numerous iron oxide/chloride phases exhibit quite close peak positions, and LAL-generated nanomaterials often contain high fractions of amorphous phase [21,26,32,44], determining the precise phase composition of the samples seems impossible. Nevertheless, in Figure 9 we show a set of the most probable phases observed in the patterns of Samples A and B, which is generally consistent with the conclusions previously drawn from XPS measurements. More specifically, both samples were based on a mixture of iron-oxide and iron-chloride phases, in which both Fe(II) and Fe(III) species coexist. Interestingly, and in agreement with previous work reported by others [33,34,37–39,50], according to the XRD patterns, the main phase with the best-detected signals could be hematite (Fe_2O_3). As was found by XPS observations, the fraction of metallic Fe inclusions was quite small, which is why one cannot see metallic Fe in the XRD patterns.

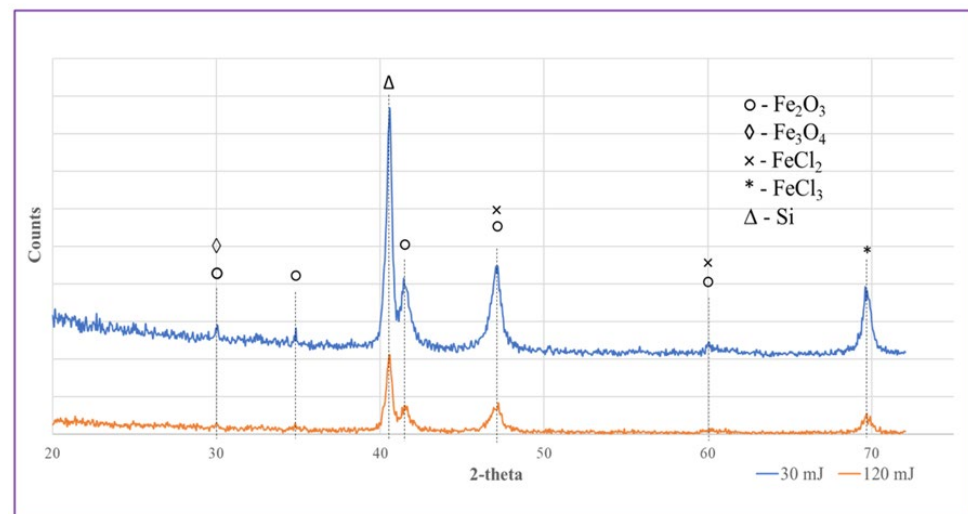


Figure 9. XRD patterns of Samples A (blue) and B (orange) prepared at 30 (blue) and 120 mJ/pulse (orange) and deposited on Si wafer.

Thus, based on the above-mentioned analyses, the NPs prepared by the LAL method, both Samples A and B, were based on a mixture of iron chloride and oxide phases, with some metallic Fe(0) species as admixture. This was expected to make such NPs release Fe ions in water when PLLA nanosheets embedded with them were immersed into physiological solution at pH 7.4.

3.4. Ion Release from NP-Loaded NSs

Optical microscopy observations of prepared PLLA NSs incorporated with NPs (both cross-sectional and surface view) demonstrated that the NPs were fairly uniformly distributed in the prepared NSs, being entrapped during spin-coating as agglomerates into pockets of different sizes formed by spin-coated PLLA NSs (see Supplementary Materials Figures S4 and S5).

As seen in Figure S4, the thickness of PLLA NSs prepared in this study was mainly between ~80 and ~100 nm, indicating that all the NPs used by us were smaller and could be incorporated into such NSs. It was found that most of loaded NPs were entrapped as

agglomerates into relatively large PLLA pockets, implying that the spin-coating process employed to prepare NSs is still to be optimized in the future in order to understand better how rotational speed, as well as concentrations of incorporated NPs and PLLA as a polymer itself, influence the thickness and morphology of prepared NSs. Meanwhile, in this study, we mainly focused on the ability of the prepared PLLA NSs to release Fe ions in contact with physiological solution.

The ion release potential of nanosheets incorporated with Fe-containing NPs was tested by means of ICP-MS, for which the NSs were immersed in a buffer solution with pH 7.4 and kept at a temperature of 37 °C, as shown in Figure 4. After certain periods of time, aliquots were taken in order to measure the concentration of released Fe (or/and) Zn ions. Figure 10 presents the results of ICP-MS measurements obtained for two PLLA NSs incorporated with Fe-containing NPs from Samples A (a) and B (b). In both cases, the prepared NSs were adjusted to incorporate comparable amounts of Fe atoms, which was controlled during spin-coating (~0.3 mg/mL of Fe in CHCl_3).

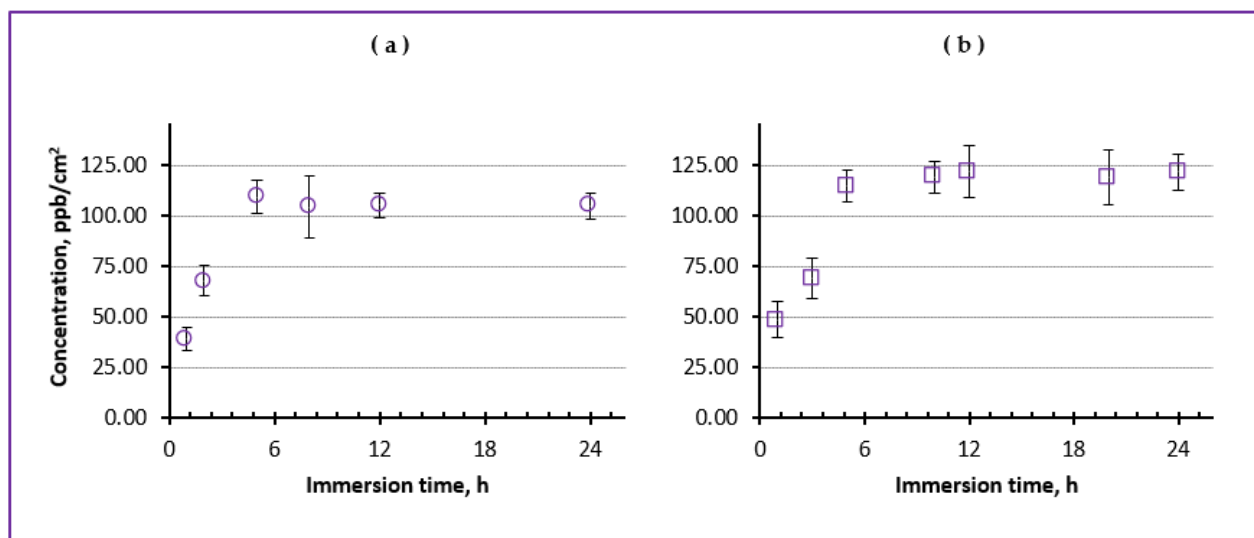


Figure 10. Concentration of Fe ions released by NSs incorporated with Fe-containing NPs laser-prepared at 30 (a) and 120 mJ/pulse (b). Both NSs were prepared using corresponding colloids with the same NP concentration (~0.3 mg/mL).

It is seen in Figure 10 that the concentration of Fe ions released by both NSs into physiological solution (pH 7.4) gradually increased during the first ~5 h of immersion into the liquid, after which the amount of released ions was quite constant for the next ~20 h of the experiment. The maximum level achieved was detected to be quite low, being on the order of just ~110 ppb/cm². However, here it should be noted that to date the optimum concentration of Fe ions on skin surface necessary to enhance burn wound healing is not known yet and still has to be determined. At the same time, the very fact that the prepared PLLA nanosheets released Fe ions from their incorporated NPs as soon as after 5 h seems very promising, as this implies that in real life such dressings can provide some Fe ions on wound surface already a few hours after their application. This seems very attractive, because typically dressings are used on wounds for as long as ~24 h before replacement, and therefore it is important for them to release their drugs or microelements within a reasonably short period of time.

For comparison, at the next stage, we also prepared NSs incorporated with both Fe and Zn ions, for which Sample B and commercial ZnO NPs were used. Figure 11 demonstrates how a PLLA NS embedded with two types of NPs released Fe (triangles) and Zn (diamonds) ions when immersed in physiological solution at pH 7.4. It is seen that different levels of concentration were achieved by Fe and Zn ions released by this NS, which was intentionally embedded with different amounts of nanoparticles. Importantly, however, the maximum

level of both Fe and Zn ions was achieved after around 4–5 h of immersion. This probably implies that it is the permeability of the PLLA NS that played an important role in releasing ions of the two types. As mentioned above, the difference in released concentration of Fe and Zn ions can be explained by the different amount of NPs used during spin-coating. Here, we used the same concentration of Sample B to prepare this NS (0.3 mg/mL of Fe in chloroform), while 1.0 mg/mL of ZnO NPs was added into the same dispersion.

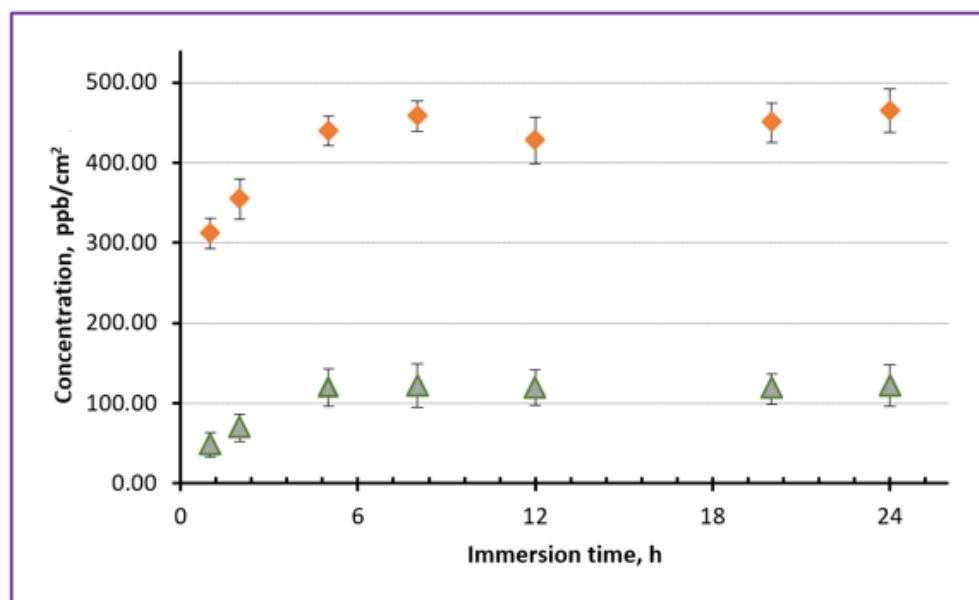


Figure 11. Concentration of Fe (triangles) and Zn (diamonds) ions released by NSs incorporated with two types of NPs. Sample B and commercial ZnO NPs (with sizes below 25 nm) were used as source of Fe and Zn ions, respectively.

At the same time, for comparison, we also used commercially available iron oxide NPs (Fe_2O_3), which were incorporated into PLLA NSs at different concentrations and then analyzed by ICP-MS after their immersion in the solution. However, no noticeable level of Fe release was observed in their case which could be detected by ICP-MS, agreeing well with the insolubility of Fe_2O_3 in water.

The main focus of this study was on preparing Fe-containing NPs that would be soluble in water and release Fe ions. This task was quite challenging, as iron oxides are known to have very low solubility in water. In addition, it should be added that thus far the level of concentration of microelements (such as Fe and Zn) desired in the wound area for efficient healing is not known yet and needs additional studies. For this reason, here we only aimed to show that (1) water-soluble Fe-containing NPs capable of releasing ions could be prepared by laser ablation and then incorporated into biodegradable NSs; (2) two types of NPs with different metal ions (Fe and Zn) could be embedded simultaneously and then release their ions over time independently. At the same time, *in vivo* tests on animals are needed to see how PLLA NSs incorporated with useful microelements can influence wound healing. However, the fact that several types of metal ion-containing NPs can be embedded into PLLA nanosheets, and that such ions are then independently released as fast as within several hours (up to 4–5), shows promise. It is obvious that wound dressings, when placed at the wound area, should demonstrate their efficacy and contribute to healing-related processes within several hours.

4. Conclusions

Burn healing is known to be accelerated by the presence of ions of certain microelements (including Fe and Zn). Aiming at developing inexpensive and easy-to-use patches for burns, in this work, we prepared biodegradable polymer nanosheets of poly(L-lactic

acid), PLLA, loaded with Fe-containing nanoparticles which were generated by means of laser ablation in chloroform as medium. Such thin PLLA nanosheets incorporated with Fe-containing nanoparticles are believed to release Fe ions in contact with skin, which should facilitate skin healing.

We first prepared water-soluble nanoparticles based on Fe ions via ablating iron plate by laser in chloroform. The method was chosen as we aimed at generating chloride/oxide-based nanomaterials which would demonstrate solubility in contact with water. The prepared nanoparticles were found to be of proper sizes (below 100 nm) and based on Fe chloride and oxide phases, which made them suitable for incorporation into PLLA nanosheets via spin-coating. After characterization, the prepared Fe-containing nanomaterials were embedded into PLLA nanosheets which were fabricated via spin-coating. To test their ion-releasing properties, the prepared nanosheets were immersed in a buffered liquid (pH 7.4) at 37 °C, where their Fe ion release was monitored over time.

In parallel, we also prepared PLLA nanosheets incorporated with two types of ions, Fe and Zn, to demonstrate that PLLA nanosheets can be loaded with reservoirs of several metal ions that are known to stimulate wound healing. Importantly, independent ion release was demonstrated by such nanosheets, with attractive ion release rates, which makes the prepared nanosheets promising for further development of biomedical materials on their bases.

Supplementary Materials: The following supporting information can be downloaded at: <https://www.mdpi.com/article/10.3390/nanomanufacturing3040025/s1>, Figure S1: XPS Cl 2p spectra of Fe-containing NPs in Samples A (a) and B (b); Figure S2: XPS O 1s spectra of Fe-containing NPs in Samples A (a) and B (b); Figure S3: Elemental composition of Samples A and B prepared by LAL (as calculated based on XPS results); Figure S4: Cross-sectional SEM images of PLLA NSs incorporated with NSs. The nanosheets were spin-coated on Si substrate and have ~190-nm-thick PVA under-layer. In upper image: 110 nm shows cross-sectional thickness of PLLA sheet; 199 nm depicts thickness of PVA layer; 149 nm stands for strained Si wafer layer formed during breakage. In lower panel: 84.8 nm is thickness of PLLA sheet, while 193 nm depicts thickness of PVA layer plus PLLA layer on it; Figure S5: Surface images (SEM micrographs) of PLLA NSs loaded with Fe-containing (b,d) and with ZnO (a,c) NPs. Scale bar indicates 1 µm.

Author Contributions: Methodology, A.M., S.I. and S.A.K.; Conceptualization, S.A.K.; Investigation, A.M., N.M., A.A.A., D.A. and S.O.G.; Formal analysis, A.M., A.A.A., S.O.G. and A.K.B.; Supervision, N.M., S.I. and S.A.K.; Project administration, S.A.K. and S.I.; Data curation, A.A.A., D.A., S.I. and S.A.K.; Writing—original draft, A.M., N.M., A.K.B. and S.A.K.; Writing—review and editing, N.M., S.I. and S.A.K. All authors have read and agreed to the published version of the manuscript.

Funding: The research was financially supported by the Russian Foundation of Basic Research (RFBR) (grant no. RFBR 20-52-04005).

Data Availability Statement: Not applicable.

Acknowledgments: The research was financially supported by the Japan Society for the Promotion of Science (JSPS) (grant no. 16K04904). S.A.K. also thanks the support from the Amada Foundation (grant no. AF-2019225-B3).

Conflicts of Interest: The authors declare no conflict of interest.

References

1. Lazurus, G.S.; Cooper, D.M.; Knighton, D.R.; Margolis, D.J.; Pecararo, R.E.; Rodeheaver, G.; Robson, M.C. Definitions and guidelines for assessment of wounds and evaluation of healing. *Arch. Dermatol.* **1994**, *130*, 489–493. [[CrossRef](#)]
2. Lin, P.H.; Sermersheim, M.; Li, H.C.; Lee, P.H.U.; Steinberg, S.; Ma, J. Zinc in wound healing modulation. *Nutrients* **2018**, *10*, 116. [[CrossRef](#)] [[PubMed](#)]
3. Cappuccio de Castro, K.; Silva, E.K.; Nogueira Campos, M.G.; Innocentini Mei, L.H. Hyaluronic acid/polyvinyl alcohol electrospun nanofiber membranes loaded with plantago major extract for smart wound dressings. *ACS Appl. Nano Mater.* **2022**, *5*, 12616–12625. [[CrossRef](#)]

4. Bandeira, M.; Chee, B.S.; Frassini, R.; Nugent, M.; Giovanela, M.; Roesch-Ely, M.; Crespo, J.S.; Devine, D.M. Antimicrobial PAA/PAH electrospun fiber containing green synthesized zinc oxide nanoparticles for wound healing. *Materials* **2021**, *14*, 2889. [[CrossRef](#)]
5. Abdollahi, Z.; Zare, E.N.; Salimi, F.; Goudarzi, I.; Tay, F.R.; Makvandi, P. Bioactive carboxymethyl starch-based hydrogels decorated with CuO nanoparticles: Antioxidant and antimicrobial properties and accelerated wound healing in vivo. *Int. J. Mol. Sci.* **2021**, *22*, 2531. [[CrossRef](#)]
6. Basit, H.M.; Ali, M.; Shah, M.M.; Shah, S.U.; Wahab, A.; Albarqi, H.A.; Alqahtani, A.A.; Walbi, I.A.; Khan, N.R. Microwave enabled physically cross linked sodium alginate and pectin film and their application in combination with modified chitosan-curcumin nanoparticles. A novel strategy for 2nd degree burns wound healing in animals. *Polymers* **2021**, *13*, 2716. [[CrossRef](#)]
7. Reczyńska-Kolman, K.; Hartman, K.; Kwiecień, K.; Brzychczy-Włoch, M.; Pamuła, E. Composites based on gellan gum, alginate and nisin-enriched lipid nanoparticles for the treatment of infected wounds. *Int. J. Mol. Sci.* **2022**, *23*, 321. [[CrossRef](#)]
8. Nawaz, T.; Iqbal, M.; Khan, B.A.; Nawaz, A.; Hussain, T.; Hosny, K.M.; Abualsunun, W.A.; Rizg, W.Y. Development and optimization of acriflavine-loaded polycaprolactone nanoparticles using box-behnken design for burn wound healing applications. *Polymers* **2022**, *14*, 101. [[CrossRef](#)]
9. Verbelen, J.; Hoeksema, H.; Heyneman, A.; Pirayesh, A.; Monstrey, S. Aquacel[®] Ag dressing versus Acticoat[™] dressing in partial thickness burns: A prospective, randomized, controlled study in 100 patients. Part 1: Burn wound healing. *Burns* **2014**, *40*, 416–427. [[CrossRef](#)]
10. He, C.H.; Yu, B.R.; Lv, Y.C.; Huang, Y.F.; Guo, J.D.; Li, L.; Chen, M.M.; Zheng, Y.Q.; Liu, M.H.; Guo, S.B.; et al. Biomimetic asymmetric composite dressing by electrospinning with aligned nanofibrous and micropatterned structures for severe burn wound healing. *ACS Appl. Mater. Interfaces* **2022**, *14*, 32799–32812. [[CrossRef](#)]
11. Ishak, M.Q.H.; Shankar, P.; Turabayev, M.E.; Kondo, T.; Honda, M.; Gurbatov, S.O.; Okamura, Y.; Iwamori, S.; Kulinich, S.A. Biodegradable polymer nanosheets incorporated with Zn-containing nanoparticles for biomedical applications. *Materials* **2022**, *15*, 8101. [[CrossRef](#)] [[PubMed](#)]
12. Li, J.; Wang, C.; Han, X.S.; Liu, S.; Gao, X.; Guo, C.L.; Wu, X.C. Aramid nanofibers-reinforced rein fibrous hydrogels as antibacterial and anti-inflammatory burn wound dressings. *ACS Appl. Mater. Interfaces* **2022**, *14*, 45167–45177. [[CrossRef](#)] [[PubMed](#)]
13. Kaul, S.; Sagar, P.; Gupta, R.; Garg, P.; Priyadarshi, N.; Singhal, N.K. Mechanobactericidal, gold nanostar hydrogel-based bandage for bacteria-infected skin wound healing. *ACS Appl. Mater. Interfaces* **2022**, *14*, 44084–44097. [[CrossRef](#)]
14. Coger, V.; Million, N.; Rehbock, C.; Sures, B.; Nachev, M.; Barcikowski, S.; Wistuba, N.; Strauss, S.; Vogt, P.M. Tissue concentrations of zinc, iron, copper, and magnesium during the phases of full thickness wound healing in a rodent model. *Biol. Trace Elem. Res.* **2019**, *191*, 167–176. [[CrossRef](#)]
15. Guo, S.; DiPietro, L.A. Factors affecting wound healing. *J. Dent. Res.* **2010**, *89*, 219–229. [[CrossRef](#)] [[PubMed](#)]
16. Kavalukas, S.L.; Barbul, A. Nutrition and wound healing: An update. *Plast. Reconstr. Surg.* **2011**, *127*, 38S–43S. [[CrossRef](#)]
17. Fujie, T.; Ricotti, L.; Desii, A.; Menciasci, A.; Dario, P.; Mattoli, V. Evaluation of substrata effect on cell adhesion properties using freestanding poly(l-lactic acid) nanosheets. *Langmuir* **2011**, *27*, 13173–13182. [[CrossRef](#)]
18. Okamura, Y.; Nagase, Y. Fabrication of bio-friendly polymer nanosheets for biomedical applications. *Trans. Mat. Res. Soc. Japan* **2014**, *39*, 379–384. [[CrossRef](#)]
19. Okamura, Y.; Nagase, Y.; Takeoka, S. Patchwork coating of fragmented ultra-thin films and their biomedical applications in burn therapy and antithrombotic coating. *Materials* **2015**, *8*, 7604–7614. [[CrossRef](#)]
20. Okamura, Y.; Kabata, K.; Kinoshita, M.; Miyazaki, H.; Saito, A.; Fujie, T.; Ohtsubo, S.; Saitoh, D.; Takeoka, S. Fragmentation of poly(lactic acid) nanosheets and patchwork treatment for burn wounds. *Adv. Mater.* **2013**, *25*, 545–551. [[CrossRef](#)]
21. Kim, M.J.; Osone, S.; Kim, T.S.; Higashi, H.; Seto, T. Synthesis of nanoparticles by laser ablation: A review. *KONA Powder Part. J.* **2017**, *34*, 80–90. [[CrossRef](#)]
22. Svetlichnyi, V.A.; Shabalina, A.V.; Lapin, I.N.; Goncharova, D.A.; Velikanov, D.A.; Sokolov, A.E. Characterization and magnetic properties study for magnetite nanoparticles obtained by pulsed laser ablation in water. *Appl. Phys. A* **2017**, *123*, 763. [[CrossRef](#)]
23. Timofeev, K.L.; Kharlamova, T.S.; Ezhov, D.M.; Salaev, M.A.; Svetlichnyi, V.A.; Vodyankina, O.V. Hydroxymethylfurfural oxidation over unsupported Pd-Au alloy catalysts prepared by pulsed laser ablation: Synergistic and compositional effects. *Appl. Catal. A* **2023**, *656*, 119121. [[CrossRef](#)]
24. Shabalina, A.V.; Svetlichnyi, V.A.; Kulinich, S.A. Green laser ablation-based synthesis of functional nanomaterials for generation, storage and detection of hydrogen. *Curr. Opin. Green Sustain. Chem.* **2022**, *33*, 100566. [[CrossRef](#)]
25. Mintcheva, N.; Subbiah, D.K.; Turabayev, M.E.; Gurbatov, S.O.; Rayappan, J.B.B.; Kuchmizhak, A.A.; Kulinich, S.A. Gas sensing of laser-produced hybrid TiO₂-ZnO nanomaterials under room-temperature conditions. *Nanomaterials* **2023**, *13*, 670. [[CrossRef](#)] [[PubMed](#)]
26. Shabalina, A.V.; Fakhruddinova, E.D.; Golubovskaya, A.G.; Kuzmin, S.M.; Koscheev, S.V.; Kulinich, S.A.; Svetlichnyi, V.A.; Vodyankina, O.V. Laser-assisted preparation of highly-efficient photocatalytic nanomaterial based on bismuth silicate. *Appl. Surf. Sci.* **2022**, *575*, 151732. [[CrossRef](#)]
27. Shankar, P.; Ishak, M.Q.H.; Padarti, J.K.; Mintcheva, N.; Iwamori, S.; Gurbatov, S.O.; Lee, J.H.; Kulinich, S.A. ZnO@graphene oxide core@shell nanoparticles prepared via one-pot approach based on laser ablation in water. *Appl. Surf. Sci.* **2020**, *531*, 147365. [[CrossRef](#)]

28. Fakhrutdinova, E.; Reutova, O.; Maliy, L.; Kharlamova, T.; Vodyankina, O.; Svetlichnyi, V. Laser-based synthesis of TiO₂-Pt photocatalysts for hydrogen generation. *Materials* **2022**, *15*, 7413. [[CrossRef](#)]
29. Gurbatov, S.O.; Modin, E.; Puzikov, V.; Tonkaev, P.; Storozhenko, D.; Sergeev, A.; Mintcheva, N.; Yamaguchi, S.; Tarasenko, N.; Chivilin, A.; et al. Black Au-decorated TiO₂ produced via laser ablation in liquid. *ACS Appl. Mater. Interfaces* **2021**, *13*, 6522–6531. [[CrossRef](#)]
30. Nemoykina, A.L.; Shabalina, A.V.; Svetlichnyi, A.V. Restoration and conservation of old low-quality book paper using aqueous colloids of magnesium oxyhydroxide obtained by pulsed laser ablation. *J. Cult. Heritage* **2019**, *39*, 42–48. [[CrossRef](#)]
31. Tarasenko, N.; Shustava, E.; Butsen, A.; Kuchmizhak, A.A.; Pashayan, S.; Kulinich, S.A.; Tarasenko, N. Laser-assisted fabrication and modification of copper and zinc oxide nanostructures in liquids for photovoltaic applications. *Appl. Surf. Sci.* **2021**, *554*, 149570. [[CrossRef](#)]
32. Honda, M.; Kondo, T.; Owashi, T.; Shankar, P.; Ichikawa, Y.; Iwamori, S.; Kulinich, S.A. Nanostructures prepared via laser ablation of tin in water. *N. J. Chem.* **2017**, *41*, 11308–11316. [[CrossRef](#)]
33. Svetlichnyi, V.A.; Shabalina, A.V.; Lapin, I.N. Structure and properties of nanocrystalline iron oxide powder prepared by the method of pulsed laser ablation. *Russ. Phys. J.* **2017**, *59*, 2012–2016. [[CrossRef](#)]
34. Shabalina, A.V.; Sharko, D.O.; Korsakova, D.R.; Svetlichnyi, V.A. Iron oxide nanopowders obtained via pulsed laser ablation, for supercapacitors. *Russ. J. Inorg. Chem.* **2020**, *65*, 271–278. [[CrossRef](#)]
35. Goncharova, D.A.; Bolbasov, E.N.; Nemoykina, A.L.; Aljulaih, A.A.; Tverdokhlebova, T.S.; Kulinich, S.A.; Svetlichnyi, V.A. Structure and properties of biodegradable PLLA/ZnO composite membrane produced via electrospinning. *Materials* **2021**, *14*, 2. [[CrossRef](#)]
36. Svetlichnyi, V.A.; Shabalina, A.V.; Lapin, I.N.; Goncharova, D.A.; Velikanov, D.A.; Sokolov, A.E. Study of iron oxide magnetic nanoparticles obtained via pulsed laser ablation of iron in air. *Appl. Surf. Sci.* **2018**, *462*, 226–236. [[CrossRef](#)]
37. Svetlichnyi, V.A.; Shabalina, A.V.; Lapin, I.N.; Goncharova, D.A.; Kharlamova, T.S.; Stadnichenko, A.I. Comparative study of magnetite nanoparticles obtained by pulsed laser ablation in water and air. *Appl. Surf. Sci.* **2019**, *467–468*, 402–410. [[CrossRef](#)]
38. Maneeratanasarn, P.; Khai, T.V.; Kim, S.Y.; Choi, B.G.; Shim, K.B. Synthesis of phase-controlled iron oxide nanoparticles by pulsed laser ablation in different liquid media. *Phys. Status Solidi A* **2013**, *210*, 563–569. [[CrossRef](#)]
39. Fazio, E.; Santoro, M.; Lentini, G.; Franco, D.; Guglielmino, S.P.P.; Neri, F. Iron oxide nanoparticles prepared by laser ablation: Synthesis, structural properties and antimicrobial activity. *Colloids Surf. A* **2016**, *490*, 98–103. [[CrossRef](#)]
40. De Bonis, A.; Lovaglio, T.; Galasso, A.; Santagata, A.; Teghil, R. Iron and iron oxide nanoparticles obtained by ultra-short laser ablation in liquid. *Appl. Surf. Sci.* **2015**, *353*, 433–438. [[CrossRef](#)]
41. Honda, M.; Goto, T.; Owashi, T.; Rozhin, A.G.; Yamaguchi, S.; Ito, T.; Kulinich, S.A. ZnO nanorods prepared via ablation of Zn with millisecond laser in liquid media. *Phys. Chem. Chem. Phys.* **2016**, *18*, 23628–23637. [[CrossRef](#)] [[PubMed](#)]
42. Kondo, T.; Sato, Y.; Kinoshita, M.; Shankar, P.; Mintcheva, N.N.; Honda, M.; Iwamori, S.; Kulinich, S.A. Room temperature ethanol sensor based on ZnO prepared via laser ablation in water. *Jpn. J. Appl. Phys.* **2017**, *56*, 080304. [[CrossRef](#)]
43. Mintcheva, N.; Yamaguchi, S.; Kulinich, S.A. Hybrid TiO₂-ZnO nanomaterials prepared by laser ablation in liquid method. *Materials* **2020**, *13*, 719. [[CrossRef](#)] [[PubMed](#)]
44. Fakhrutdinova, E.D.; Shabalina, A.V.; Gerasimova, M.A.; Nemoykina, A.L.; Vodyankina, O.V.; Svetlichnyi, V.A. Highly defective dark nano titanium dioxide: Preparation via pulsed laser ablation and application. *Materials* **2020**, *13*, 2054. [[CrossRef](#)] [[PubMed](#)]
45. Gurbatov, S.O.; Puzikov, V.; Storozhenko, D.; Modin, E.; Mitsai, E.; Cherepakhin, A.; Shevlyagin, A.; Gerasimenko, A.V.; Kulinich, S.A.; Kuchmizhak, A.A. Multigram-scale production of hybrid Au-Si nanomaterials by laser ablation in liquid (LAL) for temperature-feedback optical nosensing, light-to-heat conversion, and anticounterfeit labeling. *ACS Appl. Mater. Interfaces* **2023**, *15*, 3336–3347. [[CrossRef](#)] [[PubMed](#)]
46. Sutthavas, P.; Schumacher, M.; Zheng, K.; Habibovic, P.; Boccaccini, A.R.; van Rijt, S. Zn-loaded and calcium phosphate-coated degradable silica nanoparticles can effectively promote osteogenesis in human mesenchymal stem cells. *Nanomaterials* **2022**, *12*, 2918. [[CrossRef](#)]
47. Lopes, J.H.; Souza, L.P.; Domingues, J.A.; Ferreira, F.V.; de Alencar Hausen, M.; Camilli, J.A.; Martin, R.A.; de Rezende Duek, E.A.; Mazli, I.O.; Bertran, C.A. In vitro and in vivo osteogenic potential of niobium-doped 45S5 bioactive glass: A comparative study. *J. Biomed. Mater. Res. B* **2020**, *108B*, 1372–1387. [[CrossRef](#)]
48. Sukhorukova, I.V.; Sheveyko, A.N.; Kiryukhantsev-Korneev, P.V.; Shtansky, D.V. Kinetics of Ag⁺ ion release from TiCaPCON-Ag films: Influence of Ag content and surface roughness. *Adv. Biomater. Devices Med.* **2015**, *2*, 37–43.
49. Khare, V.; Kraupper, A.; Manton, A.; Jelacic, A.; Thunemann, A.F.; Giordano, C.; Taubert, A. Stable iron carbide nanoparticle dispersions in [Emim][SCN] and [Emim][N(CN)₂] ionic liquids. *Langmuir* **2010**, *26*, 10600–10605. [[CrossRef](#)]
50. Amendola, V.; Riello, P.; Meneghetti, M. Magnetic nanoparticles of iron carbide, iron oxide, iron@iron oxide, and metal iron synthesized by laser ablation in organic solvents. *J. Phys. Chem. C* **2011**, *115*, 5140–5146. [[CrossRef](#)]

Disclaimer/Publisher's Note: The statements, opinions and data contained in all publications are solely those of the individual author(s) and contributor(s) and not of MDPI and/or the editor(s). MDPI and/or the editor(s) disclaim responsibility for any injury to people or property resulting from any ideas, methods, instructions or products referred to in the content.